Drift wave test particle transport in reversed shear profile

Wendell Horton
Institute for Fusion Studies, University of Texas at Austin, Austin, Texas 78712

Hyoung-Bin Park and Jae-Min Kwon
Department of Physics, Korea Advanced Institute of Science and Technology, Taejon 305-701, Korea

D. Strozzi and P. J. Morrison
Institute for Fusion Studies, University of Texas at Austin, Austin, Texas 78712

Duk-In Choi
Department of Physics, Korea Advanced Institute of Science and Technology, Taejon 305-701, Korea and Korea Basic Science Institute, Taejon 305-333, Korea

(Received 24 June 1998; accepted 10 August 1998)

Drift wave maps, area preserving maps that describe the motion of charged particles in drift waves, are derived. The maps allow the integration of particle orbits on the long time scale needed to describe transport. Calculations using the drift wave maps show that dramatic improvement in the particle confinement, in the presence of a given level and spectrum of $\mathbf{E}\times\mathbf{B}$ turbulence, can occur for $q(r)$ profiles with reversed shear. A similar reduction in the transport, i.e., one that is independent of the turbulence, is observed in the presence of an equilibrium radial electric field with shear. The transport reduction, caused by the combined effects of radial electric field shear and both monotonic and reversed shear magnetic q profiles, is also investigated. © *1998 American Institute of Physics.* [S1070-664X(98)03711-2]

I. INTRODUCTION

In the reversed magnetic shear experiments on the Tokamak Fusion Test Reactor (TFTR),[1] the particle transport behaves as though a barrier to transport exists near a minimum of the safety factor, $q_{\min}$. This transport barrier persists through the course of the high-power portion of the discharge ($t \simeq 2.5-3.5$ s) and correlates with the location of a $q_{\min}$ that occurs initially at $r/a \simeq 0.35$ and subsequently decreases to $r/a \simeq 0.3$ at $t \simeq 3$ s, at which time $q(0) \simeq 3.5$ and $q_{\min} \geqslant 2$. It is reported that an interpretation of the particle transport with a diffusivity D_e without a pinch term shows a decrease in D_e by a factor of about 40 in the reversed shear region $[q'(r) < 0]$. Changes in the temperature profiles are less dramatic than those in the density profiles, although power balance studies with the transport code TRANSP[2] show a large drop in the ion thermal diffusivity. Also, the electron temperature profiles change little and χ_e decreases, at most, by a factor of 2. Explaining these changes provides a puzzle that we address in this paper.

The above results are consistent with a model of the electron thermal transport caused by ambient drift wave turbulence, where modest changes in the turbulence levels are consistent with small changes in the growth rates found in a detailed eigenmode study of Reversed Shear (RS) and Enhanced Reversed Shear (ERS) plasma.[3] Dong *et al.*[4] also find only modest changes in the Ion Temperature Gradient (ITG) and trapped electron mode growth rates induced by reverse shear. Thus, we are led to a picture in which there is a dramatic improvement in the particle confinement with reversed shear profiles, without necessarily a significant change in the turbulence level. Here we show how such a reduction in transport can be explained by considering test particle motions in a fixed level of drift wave activity.

A consequence of the reduced particle transport across the q-reversed surface is the onset of a growth of the core density and pressure gradient, which, in turn, produces a growing Shafranov shift of the core plasma. Both the increasing Shafranov shift and the increasing E_r shear reduce the drift wave growth rates. These consequences would be consistent with the change in the turbulence reported in Mazzucato *et al.*[3]

An important technique that allows the long-time integration of particle orbits is to replace the actual guiding-center orbits with those of a symplectic map, a map that has the same Hamiltonian structure as the guiding-center equations. Individual orbits obtained from the map can differ qualitatively from those obtained from the differential equations, but statistically maps tend to give correct quantitative predictions. In related studies by Park *et al.*,[5] the exact ion orbits in full toroidal geometry are followed, and these results complement the present study by maps. As a practical matter, however, only with maps can one follow orbits accurately for the 10^6 time steps required to go from the wave correlation time scale $\tau_c \sim 1/\Delta\omega \sim 10^{-5}$ s to the transport time scale of $\tau_{\rm tr} \sim a^2/D \sim 1-10$ s.

We derive maps that describe particle orbits in drift waves. These maps reveal that the improved confinement for the reversed shear profile arises from a change in the topology of islands and the concomitant persistence of invariant curves in a layer in the vicinity of the point where the shear reverses, the shearless point. Away from the shearless point, we show in Sec. II how the transport degrades to that given by the standard map. Near the shearless point, however, the

map characterizing the motion is a nontwist map (see Refs. 6–8) that possesses two parameters. For the same fluctuation spectrum we show that the transport is substantially reduced for the reversed shear profile.

Specifically, in Sec. II we derive local drift wave maps that describe the plasma transport in the vicinity of a given radial position with a given q value (or rotational transform $\sim 1/q$). Away from the shearless point, the local drift wave map possesses the form of the standard map, but at the shearless point it has the form of the *standard nontwist map* that was introduced in Refs. 6–8. In Sec. III, we derive the global drift wave map, which retains the entire radial information of the q profile. The global drift wave map is used in Secs. IV and V, where we investigate the dependence of transport upon magnetic shear and the inclusion of the radial electric field with shear. A detailed depiction of the structure of the maps in the vicinity of the shearless point is given in Sec. VI. We summarize and conclude in Sec. VII.

II. DRIFT WAVE MAPS

The physical motivation and justification for introducing a map in place of the differential equations follows from the electromagnetic (laser and microwave) scattering experiments that show a wide frequency spectrum for a fixed scattering vector $\mathbf{k}$.[9,10] Numerous experiments indicate that for each drift wave vector wave number there is a broad spectrum $n\omega_0$, $n=1,2,...,N$ of frequencies. Here ω_0 is the lowest angular frequency with substantial amplitude in the drift wave spectrum. We idealize this spectrum by taking the limit $N\to\infty$ and, furthermore, assuming phase coherence of the components. We show presently that the result of these assumptions for normal magnetic shear profiles is to produce the standard map with the well-known $\mathbf{E}\times\mathbf{B}$ diffusivity $D_E=\tilde{v}_E^2\pi/\omega_0$ for both the ions and electrons. Here, $\tilde{\mathbf{v}}_E=c\tilde{\mathbf{E}}\times\mathbf{B}/B^2$ is the drift velocity induced by turbulent fluctuation. This albeit oversimplification of the drift wave spectrum captures the essential features of the $\mathbf{E}\times\mathbf{B}$ turbulent transport in monotonic $q(r)$ profiles.

We consider an electric field that possess a radial mean part plus a fluctuating part. For the fluctuating part we use the model drift wave spectrum,

$$\tilde{\phi}(\mathbf{x},t)=\sum_{m,l,n}\phi_{m,l}\cos(m\vartheta-l\varphi-n\omega_0 t), \tag{1}$$

where $\tilde{\phi}$ is the electrostatic potential such that $\tilde{\mathbf{E}}=-\nabla\tilde{\phi}$. In this section we assume $\phi_{m,l}$ to be constant for local maps, though we will consider it as a function of θ and r for the global map in Sec. III. In Gaussian units, the guiding-center equations of motion are

$$\frac{d\mathbf{x}}{dt}=v_\parallel\frac{\mathbf{B}}{B}+\frac{c\mathbf{E}\times\mathbf{B}}{B^2}, \tag{2}$$

giving

$$\frac{dr}{dt}=-\frac{c}{B}\frac{1}{r}\frac{\partial\tilde{\phi}}{\partial\vartheta}, \tag{3}$$

$$r\frac{d\vartheta}{dt}=v_\parallel\frac{B_\vartheta}{B}+\frac{c}{B}\frac{\partial\tilde{\phi}}{\partial r}-\frac{c\bar{E}_r}{B}, \tag{4}$$

$$R\frac{d\varphi}{dt}=v_\parallel, \tag{5}$$

where $\mathbf{x}=(r,\vartheta,\varphi)$ and $\bar{E}_r$ is the equilibrium radial electric field. For electrostatic modes, $B_r=0$ and magnetic field errors are neglected. We also assumed $B\simeq B_\varphi\gg B_\vartheta$ as usual.

From Eqs. (1) and (3),

$$\frac{dr}{dt}=-\frac{c}{B}\frac{1}{r}\frac{\partial}{\partial\vartheta}\sum_{m,l,n}\phi_{m,l}[\cos(m\vartheta-l\varphi)\cos(n\omega_0 t)+\sin(m\vartheta-l\varphi)\sin(n\omega_0 t)]. \tag{6}$$

Since

$$\sum_{n=-\infty}^{+\infty}\cos(n\omega_0 t)=2\pi\sum\delta(\omega_0 t-2\pi n)$$

$$\text{and}\quad\sum_{n=-\infty}^{+\infty}\sin(n\omega_0 t)=0, \tag{7}$$

by symmetry,

$$\frac{dr}{dt}=\frac{2\pi c}{Br}\sum_{m,l,n}m\phi_{m,l}\sin(m\vartheta-l\varphi)\delta(\omega_0 t-2\pi n), \tag{8}$$

for this model spectrum, giving impulsive jumps in r at times $t_n=2\pi n/\omega_0$. The jumps imply that every correlation time τ_c the particle takes a new $\mathbf{E}\times\mathbf{B}$ step.

Now, for convenience, define the action $I\equiv(r/a)^2$, where a is the minor radius of the torus. Assuming one mode M, L dominates in Eq. (8), we have

$$\frac{dI}{dt}=\frac{2r}{a^2}\frac{dr}{dt}=\frac{4\pi c}{a^2B}M\phi_{M,L}\sin(M\vartheta-L\varphi)\times\sum_n\delta(\omega_0 t-2\pi n). \tag{9}$$

Integrating Eq. (9) over one jump and dropping the subscript on the electrostatic potential ϕ gives

$$I_{N+1}=I_N+\frac{4\pi c}{a^2B}\frac{M\phi}{\omega_0}\sin(M\vartheta_N-L\varphi_N). \tag{10}$$

Defining the relative phase $\psi\equiv M\vartheta(t)-L\varphi(t)$, from Eqs. (4) and (5) we have

$$\frac{d\psi}{dt}=M\frac{B_\vartheta}{rB}\left(v_\parallel-\frac{c\bar{E}_r}{B_\vartheta}\right)-L\frac{v_\parallel}{R}. \tag{11}$$

For ions in an H mode or an ERS-confinement mode, we need to keep $\bar{E}_r$. For electrons or ions in the L-mode drop $c\bar{E}_r/B_\vartheta\ll v_\parallel$. We ignore the term in this section and return to the E_r effect in Sec. V. Integrating Eq. (11) between the jumps in Eq. (9),

$$\psi_{N+1}=\psi_N+\frac{2\pi v_\parallel}{\omega_0}\frac{B_\vartheta}{rB}\left(M-L\,\frac{rB}{RB_\vartheta}\right)$$

$$=\psi_N+\frac{2\pi}{\omega_0}\,\frac{v_\parallel}{qR}\,(M-Lq). \tag{12}$$

We wish to write a map for I, ψ that has the form of the Standard Nontwist Map (SNM) of Refs. 6–8:

$$X_{N+1}=X_N+\alpha(1-Y_{N+1}^2),\quad Y_{N+1}=Y_N-\beta\,\sin(2\pi X_N). \tag{13}$$

Suppose we have a toroidal magnetic field with $q(r)=rB_\varphi/RB_\vartheta$ with a local minimum $q_m=q(r_m)$, $q'(r_m)=0$. Since $dq/dI=(dq/dr)(dr/dI)=0$ at r_m, q has a local minimum at $I_m=I(r_m)$. Considering the motion of a particle near r_m and Taylor expanding q about I_m yields

$$q(I)=q_m+\frac{q_m''}{2}\,(I-I_m)^2, \tag{14}$$

where $q_m''=q''(I_m)$. Substituting q from Eq. (14) into Eq. (12) yields

$$\frac{d\psi}{dt}=\frac{v_\parallel\left(M-Lq_m-\dfrac{L}{2}\,q_m''(I-I_m)^2\right)}{R\left(q_m+\dfrac{q_m''}{2}\,(I-I_m)^2\right)}. \tag{15}$$

To put $d\psi/dt$ into the form of the SNM, we Taylor expand Eq. (15) about $I=I_m$ to find

$$\frac{d\psi}{dt}=\frac{v_\parallel}{Rq_m}\left(M-Lq_m-\frac{Mq_m''}{2q_m}\,(I-I_m)^2\right). \tag{16}$$

We integrate Eq. (16) over the time step τ_c to get

$$\psi_{N+1}=\psi_N+\frac{2\pi}{\omega_0}\,\frac{v_\parallel}{Rq_m}\left(\delta-\frac{Mq_m''}{2q_m}\,(I_{N+1}-I_m)^2\right), \tag{17}$$

where $\delta\equiv M-Lq_m$. For I on the right-hand side, we choose I_{N+1} to make the map area preserving.

Introducing the variables

$$X=\frac{\psi}{2\pi},\quad Y=\left(\frac{Mq_m''}{2q_m\delta}\right)^{1/2}(I-I_m)=k(I-I_m), \tag{18}$$

we can write the map in the form of the SNM:

$$X_{N+1}=X_N+\frac{v_\parallel\delta}{Rq_m\omega_0}\,(1-Y_{N+1}^2)=X_N+\alpha(1-Y_{N+1}^2), \tag{19}$$

$$Y_{N+1}=Y_N-\left(\frac{-2\pi cM\phi}{a^2B\omega_0}\right)\left(\frac{2Mq_m''}{q_m\delta}\right)^{1/2}\sin(2\pi X_N)$$

$$=Y_N-\beta\,\sin(2\pi X_N). \tag{20}$$

All of the variables X, Y, α, and β are dimensionless. We can transform these dimensionless variables back to the physical ones by

$$\alpha=\frac{v_\parallel\delta}{Rq_m\omega_0},\quad \beta=\left(\frac{-2\pi cM\phi}{a^2B\omega_0}\right)\left(\frac{2Mq_m''}{q_m\delta}\right)^{1/2}, \tag{21}$$

$$\psi=2\pi X,\quad r^2=a^2\left(\frac{2q_m\delta}{Mq_m''}\right)^{1/2}Y+r_m^2. \tag{22}$$

Now consider the diffusion from a point r_0 near r_m. We define the diffusion coefficient D_r by

$$D_r\equiv\lim_{N\to\infty}\frac{\langle(r_N-r_0)^2\rangle}{2t_N}. \tag{23}$$

Assuming that $\epsilon\equiv|(r_N-r_0)/r_0|\ll 1$, we obtain

$$\langle(r_N^2-r_0^2)^2\rangle\simeq 4r_0^2\langle(r_N-r_0)^2\rangle, \tag{24}$$

and thus D_r is given by

$$D_r=\lim_{N\to\infty}\frac{\langle(r_N^2-r_0^2)^2\rangle}{8t_Nr_0^2}$$

$$=\lim_{N\to\infty}\frac{\langle(I_N-I_0)^2\rangle a^2}{8t_Nr_0^2}=\lim_{N\to\infty}\frac{\left\langle\left(\dfrac{Y_N}{k}+I_m-I_0\right)^2\right\rangle a^2}{8t_Nr_0^2}. \tag{25}$$

Integrating through Eq. (20),

$$Y_N=Y_0-\beta\sum_{i=0}^{N-1}\sin(2\pi X_i), \tag{26}$$

taking the average

$$\langle Y_N^2\rangle=\langle Y_0^2\rangle-2Y_0\beta\left\langle\sum_{i=0}^{N-1}\sin(2\pi X_i)\right\rangle$$

$$+\beta^2\left\langle\left(\sum_{i=0}^{N-1}\sin(2\pi X_i)\right)^2\right\rangle, \tag{27}$$

and assuming that the phase is uncorrelated between successive iterations, gives

$$\langle Y_N^2\rangle=Y_0^2+\beta^2\left\langle\sum_{i=0}^{N-1}\sin^2(2\pi X_i)\right\rangle=Y_0^2+\frac{N\beta^2}{2}. \tag{28}$$

Noting that $Y_0=k(I_0-I_m)$, it is seen that all constant terms in Eq. (25) vanish. Setting $N=\omega_0t/2\pi$, we can solve Eq. (23) for D_r:

$$D_r=\frac{N\beta^2a^2}{16tk^2r_0^2}=\frac{\pi}{2\omega_0}\left(\frac{cM\phi}{Br_0}\right)^2. \tag{29}$$

The conditions on α and β for Eq. (29) to apply must be determined numerically.

Now consider the motion of a particle near a point $r=r_*$ away from r_m. Assuming $q_*'\equiv q'(r_*)\neq 0$, to first order in $r-r_*$, we have

$$q(r)=q_*+q_*'(r-r_*). \tag{30}$$

From Eq. (8), we know that if one mode, say L,M, dominates, then

$$\frac{dr}{dt}=\frac{2\pi cM\phi}{Br}\sin\psi\sum_{n=-\infty}^{\infty}\delta(\omega_0t-2\pi n). \tag{31}$$

If we integrate over one jump, as we did to obtain Eq. (10), we obtain the Standard Twist Map (STM):

$$r_{N+1}=r_N+\frac{2\pi cM\phi}{Br_N\omega_0}\sin\psi_N, \tag{32}$$

$$\psi_{N+1}=\psi_N+\frac{2\pi v_\parallel}{q_* R\omega_0}\left(\delta-M\frac{q_*'}{q_*}(r_{N+1}-r_*)\right). \tag{33}$$

Calculating the diffusion coefficient about a point r_0 near r_* gives

$$D_r=\lim_{t\to\infty}\frac{\langle(r_N-r_0)^2\rangle}{2t}=\frac{\pi}{2\omega_0}\left(\frac{cM\phi}{Br_0}\right)^2, \tag{34}$$

which is the same D_r as in Eq. (29). The conditions for the onset of diffusion are different, but once diffusion sets in the diffusivity is the same, regardless of whether or not the q profile a has vanishing derivative.

III. THE GLOBAL MAP

The standard twist and nontwist maps derived above are local maps that apply in the neighborhoods of points with the characteristic features of the rotational transform selected for the expansion. When maps are advanced far into the future, however, the particle may leave these local neighborhoods. Thus, it is of considerable practical importance to write global maps, even if qualitative in terms of the particle trajectories in the true tokamak system, that describe the particle orbits for all $r/a\leqslant 1$.

The problem we wish to address is the particle transport barrier in the RS and ERS experiments. In the reversed magnetic shear experiment the particles act as though there were a barrier at the edge of the reversal region.[1] Within the context of a model, we will show that it is the nonmonotonicity of the $1/q(r)$ profile, resulting from the hollow current profiles, that causes, generically, a particle transport barrier. We show this phenomenon here without changing the fluctuation level for the onset condition for a transport barrier. The basic reason for the change in the nature of the transport is the change in the particle–wave phase relation at the $q_{\min}$ surface. The same type of effect occurs when certain conditions are met with shear in the E_r profile. Whether or not the magnetic or electric field shear profiles dominate, depends on the species and pitch angle of the particles.

For the global map, in order to determine the spatial variation of the mode amplitude $\phi_{m,l}$, we adapt the model of Connor and Taylor[11] for drift waves in toroidal geometry. In their model, electrostatic drift wave fluctuations of frequency ω_0 are given by

$$\tilde{\phi}(r,\vartheta,\varphi)=\tilde{\phi}_0\sum_m \exp[\sigma_1(x-m)^2/2]\cdot\cos[-\sigma_R(x-m)^2/2 -(m+M)\vartheta+L\varphi-\omega_0 t], \tag{35}$$

where $\tilde{\phi}_0$ is the mode amplitude, σ_R and σ_1 are real and imaginary parts of σ, $x=k\rho s$, $k=Lq/r$, $\rho=r-r_0$ is the radial distance from the rational surface given by $M=Lq(r_0)$, and $s(r)\equiv(r/q)(dq/dr)$ is the magnetic shear function.

In Eq. (35) we choose σ as $\sigma=(\omega_*/\omega_0)(\epsilon_c/bs)$ for the fluctuation in the positive shear region and as $\sigma=(\omega_*/\omega_0)\times(\epsilon_c/bs)$ for that in the negative shear region in order to represent outgoing waves propagating away from their rational surfaces. Thus, $\sigma_1<0$ gives a convergent sum in Eq. (35) in both cases. Here, the diamagnetic frequency $\omega_*=(kcT_e)/(eBL_n)$, L_n is the density scale length, $\epsilon_c=L_n/(qR_0\tau)$, R_0 is the major radius of magnetic axis, $\tau=T_e/T_i$, $b=k^2\rho_i^2$, and ρ_i is the ion gyroradius.

Assuming the same spatial variation of the mode amplitude in Eq. (35) for the whole frequency spectrum $n\omega_0$, we can get from Eqs. (3)–(5), the global map:

$$I_{N+1}=I_N+\frac{4\pi c}{\omega_0 a^2 B}\frac{\partial\tilde{\phi}}{\partial\theta}, \tag{36}$$

$$\vartheta_{N+1}=\vartheta_N+\frac{2\pi}{R\omega_0}\left(\frac{v_\parallel}{q(I_{N+1})}+\frac{2cR}{a^2B}\frac{\partial\tilde{\phi}}{\partial I}(I_{N+1})\right), \tag{37}$$

$$\varphi_{N+1}=\varphi_N+\frac{2\pi v_\parallel}{R\omega_0}. \tag{38}$$

Tracking the particle dynamics with the map rather than with the differential equations, allows us to effect long time ($\Delta t\sim 1$ s) integration. Integration on this time scale would be prohibitive with the differential equations given in Park *et al.*[5]

IV. MAGNETIC SHEAR DEPENDENCE OF TRANSPORT

We now investigate numerically the transport properties of ions by integrating the drift wave map, Eqs. (36)–(38), for the model fluctuations of Eq. (35), together with the Monte Carlo Coulomb collisional pitch angle scattering.

Assuming that small angle Coulomb scattering changes the direction, but not the magnitude, of the velocity, the collisional scattering operator for the change of the velocity variables was derived in Ref. 5:

$$(\rho_\parallel)_f=(\rho_\parallel)_i\cos\gamma+\sqrt{\frac{2\mu_i}{B_i}}\sin\gamma\cos\alpha, \tag{39}$$

$$\frac{2\mu_f}{B_f}=\left((\rho_\parallel)_i^2+\frac{2\mu_i}{B_i}\right)\sin^2\gamma\sin^2\alpha +\left(\sqrt{\frac{2\mu_i}{B_i}}\cos\gamma-(\rho_\parallel)_i\sin\gamma\cos\alpha\right)^2. \tag{40}$$

Here, $\rho_\parallel\equiv v_\parallel/\Omega_i$, Ω_i is the ion gyrofrequency at the magnetic axis, and $\mu\equiv mv_\perp^2/2B$ is the magnetic moment. In Eqs. (39)–(40), subscripts i and f refer to the initial and final values, respectively. Two angles α and γ are determined from two random numbers η_1 and η_2 on [0,1] as

$$\alpha=2\pi\eta_1,\quad \gamma=[-\nu\delta t\ln(1-\eta_2)]^{1/2}, \tag{41}$$

where ν is collision rate and $\nu\delta t\ll 1$ is required.

We have performed simulations for the TFTR and Texas Experimental Tokamak (TEXT)[12] system parameters. For the Levinton *et al.*[1] discharge in TFTR, we use $R=260$ cm, $a=90$ cm, and $B=4.6$ T. For TEXT we use ma-

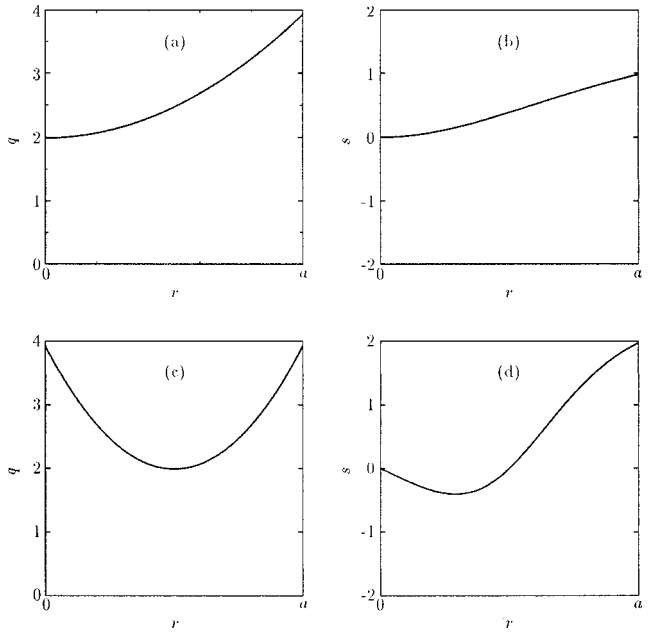

FIG. 1. Radial profiles of safety factor $q(r)$ and shear $s(r)\equiv r/qdq/dr$ for normal [(a) and (b)] and reversed [(c) and (d)] shear cases.

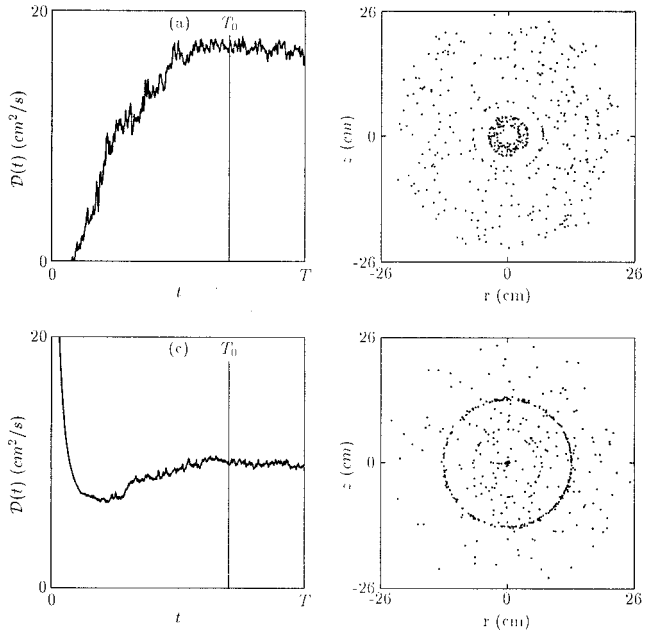

FIG. 2. Time dependences of the running diffusion coefficients and the location of particles on the poloidal section at the last moment of simulation for normal [(a) and (b)] and reversed [(c) and (d)] shear cases.

jor radius $R_0=100$ cm, minor radius $a=26$ cm, and centerline field $B=3$ T. The results are qualitatively similar for the same q profiles. While TEXT did not operate in the RS regime, our earlier study[5] of transport used TEXT parameters. Two q profiles, the normal $q(r)=1.99+1.94(r/a)^2$ and the reversed $q(r)=1.99+7.76(r/a-0.5)^2$, are used (see Fig. 1). We choose $\omega_0=1.93\times10^5$, $L=6$, $M=15$, $L_n/R_0=0.2$, and $\delta=0.5$, which do not contradict the assumptions for Eq. (35).

In Fig. 2 we show the time dependences of the running diffusion coefficients,

$$\mathscr{D}(t)=\frac{1}{2t}\frac{1}{N}\sum_{j=1}^{N}[r_j(t)-r_j(0)]^2, \tag{42}$$

for an ensemble of D^+ ions composed of 1024 passing particles that initially have $r=2-7.2$ cm for core ions and random ϑ's with the kinetic energy $\mathscr{E}=1$ keV and $\lambda\equiv\mu/\mathscr{E}=1\times10^{-9}$ with $\widetilde{\phi_0}=0.3$ eV and $\nu=1\,s^{-1}$. The integration time step is $0.1\times2\pi/\omega_0\simeq3.26$ μs and total integration time T is 10^6 time steps.

The running diffusion coefficients converge to well-defined constant values, indicating that the radial transport is a diffusion process. We can obtain the diffusion coefficient from the time series of $\mathscr{D}(t)$ as

$$\overline{\mathscr{D}}=\frac{1}{T-T_0}\int_{T_0}^{T}\mathscr{D}(t)dt, \tag{43}$$

where T_0 is the time at which convergence is observed to set in.

The diffusion coefficient is smaller for the reversed shear case, and it can be seen that the radial position of the minimum shear acts as a barrier to radial transport in that case. This shows that the change in the particle–wave phase relation at the minimum-q surface induces the change in the nature of the transport.

V. ELECTRIC SHEAR DEPENDENCE OF TRANSPORT

A decorrelation of the drift wave fluctuations with the plasma, which is similar to that induced by the reversed magnetic shear, also occurs if the shear in the E_r profile is large enough. For $|v_\parallel|<c|\overline{E}_r/B_\vartheta|$, the rotation in ϑ is dominated by the E_r profile, rather than by the magnetic shear. Evidently, in Eq. (37) we should replace the ϑ with

$$\vartheta_{N+1}=\vartheta_N+\frac{2\pi}{\omega_0 R}\left[\frac{v_\parallel}{q(I_{N+1})}+\frac{2cR}{Ba^2}\times\left(\frac{\partial\tilde{\phi}}{\partial I}(I_{N+1})-\overline{E}_I(I_{N+1})\right)\right]. \tag{44}$$

In Fig. 3 we present the running diffusion coefficients in the presence of E_r by solving Eqs. (36), (38), and (44) for the ensemble and system parameters used in the calculations of Fig. 2. The normal q profile of Fig. 1(a) is used. The integration time step is $0.2\times2\pi/\omega_0\simeq6.51$ μs and the total integration time T is 10^6 time steps. We use two equilibrium potentials for this calculation, in order to show the effect of shear on the $\mathbf{E}\times\mathbf{B}$ poloidal velocity generated by E_r. In the first case, $\Phi_{01}(r)=-\Phi_0(1-(r/a)^2)$, which induces $v_p/r=c\overline{E}_r/(rB_t)\sim1+\epsilon$; i.e., the profile induces small shear in the $\mathbf{E}\times\mathbf{B}$ poloidal velocity. In contrast, the second equilibrium potential $\Phi_{02}=-\Phi_0(1-(r/a)^2)\exp(1-r/a)$, results in a strongly sheared v_p/r profile.

For Φ_{01}, which has little shear, the diffusion coefficient is not much different from that of the no E_r case of Fig. 2(a). In contrast, the results for Φ_{02} shows that E_r generates enough shear in the $\mathbf{E}\times\mathbf{B}$ poloidal velocity to suppress the transport induced by the drift wave electrostatic fluctuations, as first proposed by Biglari *et al.*[13] and numerically confirmed for the global toroidal system in Ref. 5 by solving the

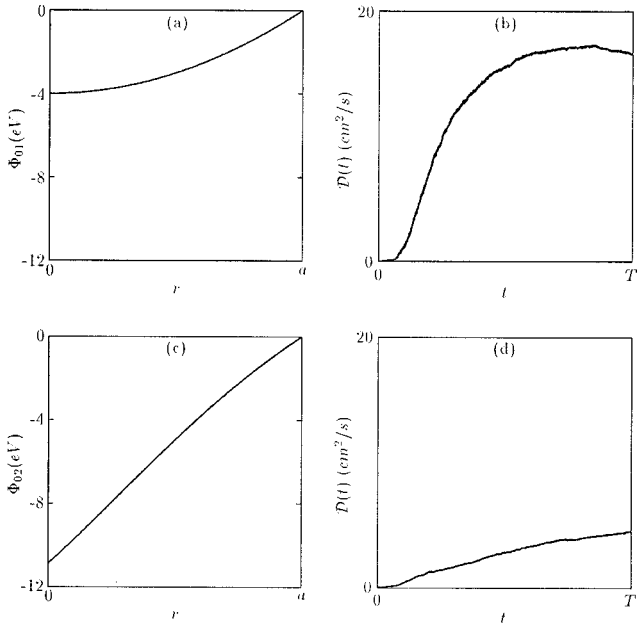

FIG. 3. Radial profiles of equilibrium potential and running diffusion coefficients for Φ_{01} [(a) and (b)] and Φ_{02} [(c) and (d)] in normal q equilibrium.

coupled ordinary differential equations for the exact guiding-center trajectories. When we use the E_r profiles in Fig. 3 in the reversed q equilibrium, we get diffusion coefficients, each of which is smaller than their counterparts in Fig. 3.

For $|v_\parallel| \sim c|E_r/B_\vartheta|$ the rotation in ϑ is induced by both the q and E_r profiles, and the relative direction of rotation generated by the magnetic and electric shear is important. The rotation components might add up, or compensate each other, as can be easily seen in Eq. (44). In Fig. 4 we present the running diffusion coefficients in the presence of E_r with the reversed q profile given in Fig. 1(c) by solving Eqs. (36), (38), and (44). The ensemble and system parameters used in these calculations are the same as those of Fig. 2. The integration time step is $0.2\times 2\pi/\omega_0 \simeq 6.51\ \mu$s and the total integration time T is 10^6 time steps. In the first case, $\Phi_{03}(r) = \Phi_0[1-(1-2r/a)^2]$, which induces $v_p/r = cE_r/(rB_t) > 0$ for $r < a/2$, and vice versa. In this case with $\Phi_0 = 1$ keV, the electric field induces poloidal velocity in the opposite direction to that induced by the magnetic shear, and the diffusion coefficient is larger than that of Fig. 2(c) for the case without a radial electric field. In contrast, $\Phi_{04} = \Phi_0(1-2r/a)^2$ induces $v_p/r = cE_r/(rB_t) < 0$ for $r < a/2$, and vice versa. In this case the diffusion coefficient is smaller than that of Fig. 2(c).

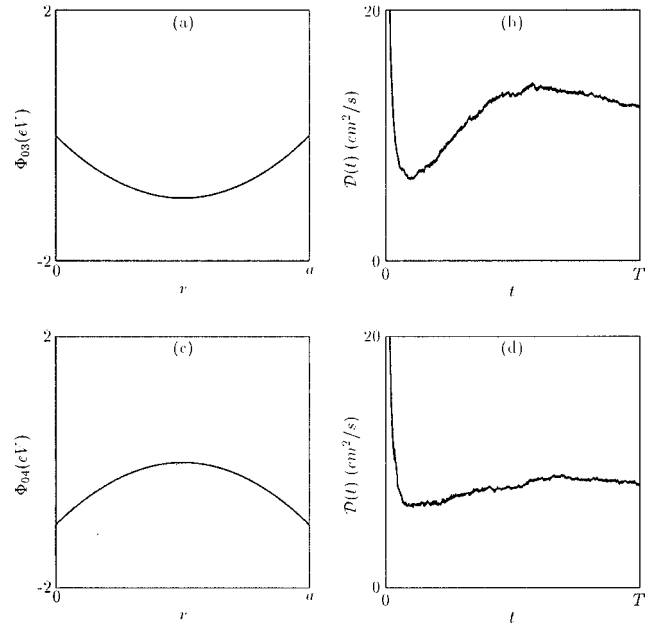

FIG. 4. Radial profiles of equilibrium potential and running diffusion coefficients for Φ_{03} [(a) and (b)] and Φ_{04} [(c) and (d)] in reversed q equilibrium.

VI. MAP STRUCTURES IN A REVERSED SHEAR PLASMA

To isolate the effects of reversed shear and radial electric field profiles from those of the radial variation of mode amplitude, random noise of collisions, and others, we consider the simple global map, including a single mode of, M,L, with no radial variation of the mode amplitude. We solve the following mapping equation, which is similar to Eqs. (10) and (12), but includes the effect of an equilibrium radial electric field:

$$I_{N+1} = I_N + \frac{4\pi c}{a^2 B_0}\frac{M\phi}{\omega_0}\sin(M\vartheta_N - L\varphi_N), \tag{45}$$

$$X_{N+1} = X_N + R_1(I_{N+1}) + R_2(I_{N+1}), \tag{46}$$

$$R_1(I) = \frac{v_\parallel(I)}{\omega_0 qR}\,[M - Lq(I)], \tag{47}$$

$$R_2(I) = -\frac{cM}{\omega_0 a B_0}\frac{\overline{E}_r(I)}{\sqrt{I}}, \tag{48}$$

$$v_\parallel(I) = \sqrt{\frac{2}{m}\,[\mathcal{E}_t - e\Phi_0(I)](1-\lambda B_0)}. \tag{49}$$

Here the equilibrium radial electric field $\overline{E}_r(I) = -\partial\Phi_0/\partial r|_{r=a\sqrt{I}}$, the initial total energy is $\mathcal{E}_t$, and e is the charge of the particle considered. We investigate the map phase space structure by calculating particle trajectories with various initial conditions in configuration space, for the reversed shear case above. In Figs. 5 and 6 we present the map phase space for cases with $\mathcal{E}_t = 167$ and 370 eV, which were chosen to make the denominator of the major rational rotation number near the minimum q surface be odd and even integers for each case. In the case of Fig. 5 the surface with the rotation number 1 is located near the minimum q surface, and in the case of Fig. 6 the surface with the rotation number $\frac{3}{2}$ exists. All the other parameters are same as those used in the calculations of Figs. 2(c)–2(d). In these calculations we do not consider the equilibrium electric field. Figures 5 and 6 show the role of the minimum q surface, i.e., the shearless curve, in producing a transport barrier, and the typical separatrix reconnection of odd-period and even-period orbits of the SNM (see Ref. 7). We show the rotation number profiles for both cases in Fig. 7.

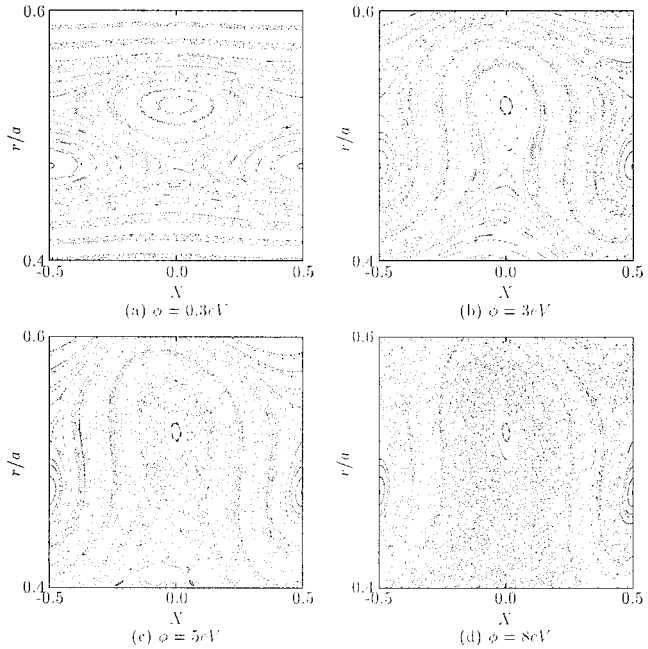

FIG. 5. The surface of section for the structures in the map in Eqs. (45)–(49). The drift wave potential amplitudes are (a) $\phi=0.3$ eV, (b) $\phi=3$ eV, (c) $\phi=5$ eV, and (d) $\phi=8$ eV in the case that a period-odd orbit exists near the shearless curve of a minimum-q surface.

To see the modification of the rotation number profile due to the radial electric field, we consider the model electric field,

$$\overline{E}_r = -\frac{0.6rE_0}{a\left[1+80\left(\frac{r^2}{a^2}-0.8\right)^2\right]}. \tag{50}$$

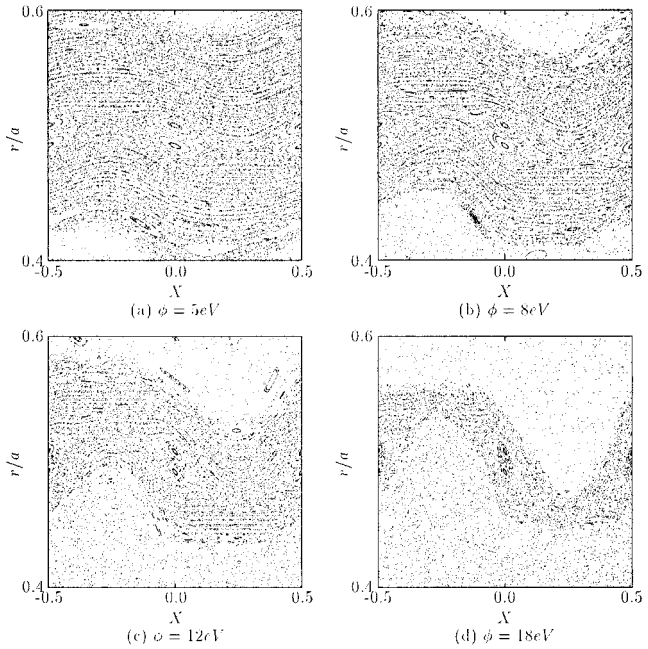

FIG. 6. Map structures for (a) $\phi=5$ eV, (b) $\phi=8$ eV, (c) $\phi=12$ eV, and (d) $\phi=18$ eV in the case that a period-even orbit exists near the shearless curve of a minimum-q surface.

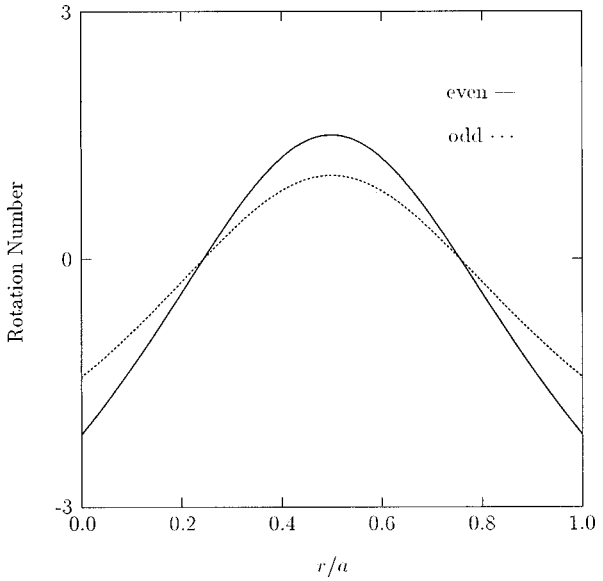

FIG. 7. Rotation number profiles for the cases in Figs. 5 and 6.

The magnitude of above radial electrostatic potential (aE_0) is a few keV, which is enough to appreciably modify the rotation number profile. The resultant total rotation number profile has three extremum surfaces, as shown in Fig. 8(b). All of these surfaces act as confinement barriers, as can be seen in Fig. 8(d). We used $\phi=6$ eV and $\mathscr{E}_t=1$ keV for this calculation. Observe that the transport is suppressed where the total rotation number profile R_1+R_2 is shearless, which is a universal property in area preserving nontwist maps.[7]

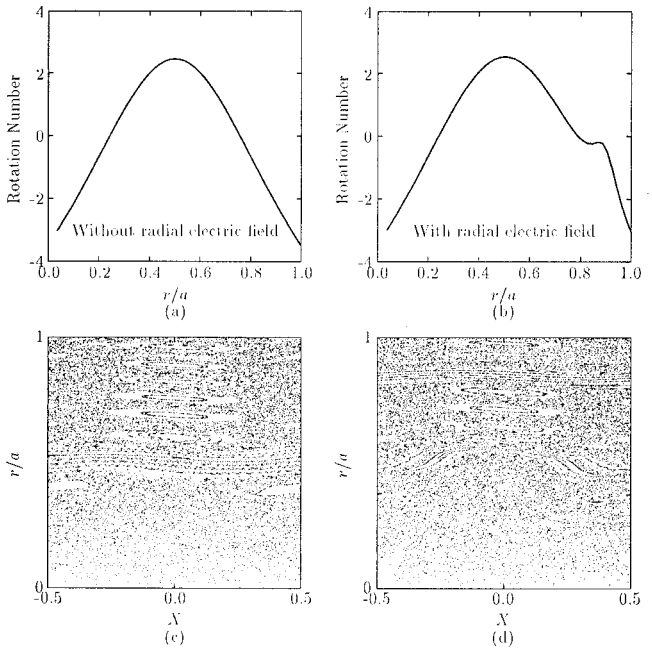

FIG. 8. Rotation number profiles and the surface of section for the map structures without (a) and (c) and with (b) and (d) a radial electric field in Eq. (50).

VII. CONCLUSIONS

We derived the drift wave maps to allow the integration of orbits on the long transport time scales, which is practically impossible for the differential equations governing the exact guiding-center orbits. Calculations using the drift wave map showed that a dramatic improvement in the particle confinement, in the presence of **E×B** turbulence, can occur for reversed shear $q(r)$ profiles, without necessarily a significant change in the turbulence level.

The improved confinement results from the change in the form (topology) of the invariant torii associated with the nonmonotonic winding number in the area preserving map. The conditions for the presence of a barrier involve both the dimensionless wave amplitude parameter β and the phase parameter α of the standard nontwist map. We show that once the β parameter is large enough for the onset of diffusion across the $q_{\min}$ surface, the diffusivity is exactly the same value as that obtained for the chaotic regime of the standard map, which applies in the case of monotonic (normal) q profiles. Similar results exist in the case of combined E_r shear and reversed shear q profiles when account is taken of the actual rotation number profile for the transport of particles with a specified kinetic energy, pitch angle, and charge-to-mass ratio (species).

A change in the particle-to-drift wave fluctuation phase relation, similar to that induced by reversed magnetic shear, also occurs if the shear in the $\overline{E}_r$ profile is large enough. For $|v_\parallel| \equiv c|\overline{E}_r/B_\vartheta|$, the rotation in ϑ is induced by both q and E_r profiles, and the relative direction of the phase rotation generated from magnetic and electric shear is important. The two rotational components might add up, or compensate each other, as shown in the examples.

ACKNOWLEDGMENTS

This work was supported by the U.S. Department of Energy Contract No. DE-FG03-96ER-54346, and by the Korea Advanced Institute for Science and Technology. One of us (DS) was supported by the U.S. Department of Energy undergraduate Fellowship in Plasma Physics and Fusion Engineering.

[1] F. M. Levinton, M. C. Zarnstorff, S. H. Batha, M. Bell, R. E. Bell, R. V. Budny, C. Bush, Z. Chang, E. Fredrickson, A. Janos, J. Manickam, A. Ramsey, S. A. Sabbagh, G. L. Schmidt, E. J. Synakowski, and G. Taylor, Phys. Rev. Lett. **75**, 4417 (1995).
[2] R. Budny, M. G. Bell, H. Biglari, M. Bitter, C. Bush, C. Z. Cheng, E. Fredrickson, B. Grek, K. W. Hill, H. Hsuan, A. Janos, D. L. Jassby, D. Johnson, L. C. Johnson, B. LeBlanc, D. C. McCune, D. R. Mikkelsen, H. Park, A. T. Ramsey, S. A. Sabbagh, S. Scott, J. Schivell, J. D. Strachan, B. C. Stratton, E. Synakowski, G. Taylor, M. C. Zarnstorff, and S. J. Zweben, Nucl. Fusion **32**, 429 (1992).
[3] E. Mazzucato, S. H. Batha, M. Beer, M. Bell, R. V. Budny, C. Bush, T. S. Hahm, G. W. Hammett, F. M. Levinton, R. Nazikian, H. Park, G. Rewoldt, G. L. Schmidt, E. J. Synakowski, W. M. Tang, G. Taylor, and M. C. Zarnstorff, Phys. Rev. Lett. **77**, 3145 (1996).
[4] J. Q. Dong, S. M. Mahajan, and W. Horton, Phys. Plasmas **4**, 755 (1997).
[5] H-B. Park, E-G. Heo, W. Horton, and D-I. Choi, Phys. Plasmas **4**, 3273 (1997).
[6] D. del-Castillo-Negrete and P. J. Morrison, Phys. Fluids A **5**, 948 (1993).
[7] D. del-Castillo-Negrete, J. M. Greene, and P. J. Morrison, Physica D **91**, 1 (1996).
[8] D. del-Castillo-Negrete, J. M. Greene, and P. J. Morrison, Physica D **100**, 311 (1997).
[9] D. L. Brower, W. A. Peebles, N. C. Luhmann, Jr., and R. L. Savage, Jr., Phys. Rev. Lett. **54**, 689 (1985).
[10] E. Mazzucato and R. Nazikian, Phys. Rev. Lett. **71**, 1840 (1993).
[11] J. W. Connor and J. B. Taylor, Phys. Fluids **30**, 3180 (1987).
[12] K. W. Gentle, Nucl. Technol. Fusion **1**, 479 (1981).
[13] H. Biglari, P. H. Diamond, and P. W. Terry, Phys. Fluids B **2**, 1 (1990).